Multimode Strong Coupling in Superconducting Cavity Piezoelectromechanics

Xu Han, Chang-Ling Zou, and Hong X. Tang*
Department of Electrical Engineering, Yale University, New Haven, Connecticut 06511, USA
(Received 21 April 2016; published 14 September 2016)

High-frequency mechanical resonators subjected to low thermal phonon occupancy are easier to be prepared to the ground state by direct cryogenic cooling. Their extreme stiffness, however, poses a significant challenge for external interrogations. Here we demonstrate a superconducting cavity piezoelectromechanical system in which multiple modes of a bulk acoustic resonator oscillating at 10 GHz are coupled to a planar microwave superconducting resonator with a cooperativity exceeding 2×10^3, deep in the strong coupling regime. By implementation of the noncontact coupling scheme to reduce mechanical dissipation, the system exhibits excellent coherence characterized by a frequency–quality-factor product of 7.5×10^{15} Hz. Interesting dynamics of classical temporal oscillations of the microwave energy is observed, implying the coherent conversion between phonons and photons. The demonstrated high-frequency cavity piezoelectromechanics is compatible with superconducting qubits, representing an important step towards hybrid quantum systems.

DOI: 10.1103/PhysRevLett.117.123603

Introduction.—Controlling mechanical motion by an electromagnetic field has recently emerged as a new field of great interest [1–3]. Impressive progress has been achieved in various cavity electromechanical and optomechanical systems, including ground-state cooling of mechanical resonators [4–6], quantum squeezing of a mechanical mode [7,8], and efficient conversion between photons at vastly different frequencies [9–11]. To realize coherent quantum operations, the mechanical resonator needs to be prepared in the ground state and the photon-phonon coupling rate must overcome the energy dissipation rate of each individual system to its local environment, reaching the so-called strong coupling regime [12–15]. For this reason, realizing strong coupling in a high-frequency mechanical system is desirable since higher mechanical resonant frequency (ω_m) translates to a lower thermal phonon occupation number ($\bar{n} \approx k_B T/\hbar\omega_m$, where k_B is the Boltzmann constant, T is the temperature, $\hbar$ is the reduced Planck constant) and hence eases refrigeration conditions for reaching the ground state ($\bar{n} \ll 1$). Particularly, mechanical resonators above ~10 GHz can be cooled to ground state by direct dilution refrigeration without the necessity of active cooling techniques such as feedback cooling [16,17] and sideband cooling [4,5,18].

From this perspective, great efforts have been dedicated to realizing coherent cavity electromechanical and optomechanical coupling in the high-frequency regime [19–25]. One remarkable breakthrough in experiment has been achieved by the Cleland group [20], who demonstrated the ground state cooling of a 6-GHz piezoelectric bulk acoustic resonator (BAR) and the interrogation of its quantum states with a superconducting phase qubit. However, the potential of this important class of high-frequency mechanical systems can only be fully explored if its quality factor (Q factor) is further improved; even though the intrinsic Q factor of the mechanical resonator in principle can exceed 10^5, the demonstrated Q is only 260 and the phonon lifetime is limited to 6 ns in Ref. [20]. Furthermore, the wavelength of the phonon at 10 GHz is more than 4 orders of magnitude smaller than that of the microwave photon. This allows not only the reduction of the device footprint but also the study of multimode physics beyond the single mode limitation in usual microwave resonators, where a wealth of new phenomena emerges [26–30].

In this Letter, we demonstrate a high-Q superconducting cavity electromechanical system operating at 10 GHz in which a planar superconducting microwave resonator is placed over an aluminum nitride-on-silicon (AlN-on-Si) BAR in a noncontact configuration. By harnessing the strong piezoelectric effect of AlN [22,23,31], we are able to strongly couple the microwave mode with an array of acoustic thickness modes of the BAR simultaneously. Because of the non-contact-electrode coupling scheme, our system exhibits a high mechanical quality factor of 7.5×10^5 and a high frequency–quality-factor product (fQ) of 7.5×10^{15} Hz at 1.7 K, improving the phonon lifetime to 11 μs at 10 GHz. Benchmark phenomena of a strongly coupled system including avoided crossing spectra and coherent temporal oscillations are observed, featuring a high cooperativity of $C \approx 2178$. Although our experiments are conducted at 1.7 K, further refrigeration to millikelvins would bring this high-performance multimode system to the quantum regime, providing a new route for studying the complex quantum dynamics [32,33].

Cavity piezoelectromechanical coupling.—The piezoelectric interaction can be characterized by the extra electric energy due to the strain induced polarization

$H_{\text{piezo}} = \int(\Delta\mathbf{P}\cdot\mathbf{E})dV = \int[(\mathbf{e}\cdot\mathbf{S})\cdot\mathbf{E}]dV$, where $\mathbf{P}$ and $\mathbf{E}$ are the electric polarization and the electric field vectors in the material, respectively, $\mathbf{S}$ is the second-rank strain tensor, and $\mathbf{e}$ is the third-rank piezoelectric coefficient tensor of the material. In contrast to other electromechanical coupling mechanisms, such as capacitive coupling and electrostriction where the interaction depends on $|\mathbf{E}|^2$, the piezoelectric effect provides direct linear coupling between the electrical field and the mechanical motion, which in the following we refer to as "piezoelectromechanical" coupling.

To illustrate the concept of cavity piezoelectromechanical coupling, we consider a piezoelectric film BAR sandwiched between the parallel capacitor plates of an "inductor-capacitor" (LC) resonator [Fig. 1(a)]. Thickness modes of the BAR form standing longitudinal acoustic waves with the mechanical displacement sinusoidally distributed in the z direction [orange lines in Fig. 1(a)]. Because of the piezoelectric effect, the oscillating voltage on the capacitor will compress and expand the film, thus actuating the mechanical motion; conversely, the strain in the film will induce excess electric polarization in the dielectric, hence, producing oscillating voltage and current in the LC resonator. It should be noted that the coupling between the LC resonator and the piezoelectric BAR does not require electrodes to have direct contact with the BAR. In fact, contactless coupling is preferred because contacting metals and metal-dielectric interfaces are known to cause mechanical dissipation [34,35]. The elimination of metal from piezoelectric structures also allows the construction of high-Q optomechanical resonators without metal induced light absorption, making it possible to simultaneously couple acoustic modes to both microwave and optical photons for realizing microwave-to-optical conversions [3,21].

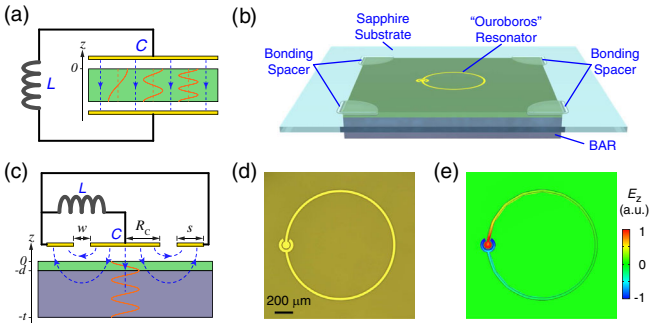

FIG. 1. (a) An illustrative configuration of a cavity piezoelectromechanical system where a piezoelectric BAR (green) is sandwiched between the parallel capacitor plates (yellow) of an LC resonator. Blue dashed lines: The electric field lines. Orange lines: Amplitude distributions of the z-component mechanical displacement of different orders of acoustic thickness modes (only the first 3 orders of modes are drawn). (b) A schematic of the piezoelectromechanical device (not to scale). The planar superconducting LC resonator ("Ouroboros") on a fabricated sapphire substrate is flipped over and suspended on top of the BAR which consists of a thin aluminum nitride layer (green) deposited on top of a thick oxidized high-resistivity silicon substrate. (c) A cross-sectional view of the device with the inductor of the Ouroboros indicated as an equivalent circuit. The device parameters are as following: $R_C = 40\ \mu$m, $s = 30\ \mu$m, $w = 10\ \mu$m, $d = 550$ nm, $t = 500\ \mu$m. (d) An optical micrograph of the Ouroboros resonator. The long arc-shaped inductor wire has a width of 25 μm and an average bending radius of 593 μm. (e) Simulated mode profile of perpendicular electric field (E_z) of the Ouroboros.

The linear piezoelectromechanical system can be described by a Hamiltonian of coupled modes under the rotating-wave approximation as

$$H/\hbar = \omega_a a^\dagger a + \sum_n \omega_{bn} b_n^\dagger b_n + \sum_n g_n(a^\dagger b_n + a b_n^\dagger), \quad (1)$$

where $a(a^\dagger)$ and $b_n(b_n^\dagger)$ are the annihilation (creation) operators for microwave photons at frequency ω_a and phonons of the nth order mechanical mode at frequency ω_{bn}, respectively, and g_n is the coupling strength between them. In this work, we focus on acoustic thickness modes with the zz-component strain (S_{zz}) piezoelectrically coupled to the z-component electric field (E_z). Then g_n can be expressed as [36]

$$g_n = \frac{e_{33}}{2\sqrt{\epsilon_0\rho}}\sqrt{\frac{\omega_a}{\omega_{bn}}}\int_{V_{\text{piezo}}} \zeta_z(\mathbf{r})\frac{\partial}{\partial z}\xi_{nz}(\mathbf{r})dV, \quad (2)$$

where e_{33} is the 33 component of the piezoelectric coefficient under the contracted Voigt notation, ϵ_0 is the vacuum permittivity, and ρ is the mass density of the mechanical resonator. ζ_z and ξ_{nz} are the z components of the normalized electric mode profile $\boldsymbol{\zeta}(\mathbf{r})$ and the mechanical displacement mode profile $\boldsymbol{\xi}(\mathbf{r})$ satisfying $\int\epsilon_r(\mathbf{r})|\boldsymbol{\zeta}(\mathbf{r})|^2dV = 1$ and $\int|\boldsymbol{\xi}_n(\mathbf{r})|^2dV = 1$, respectively, with ϵ_r being the relative dielectric constant. The integral takes place within the volume of the piezoelectric material V_{piezo}. By carefully engineering the cavity and the BAR structures to optimize the piezoelectric mode overlap, strong electromechanical coupling between the microwave mode and acoustic thickness modes is feasible [36,37].

Device design.—Since the free spectral range (FSR) of the thickness modes is inversely proportional to the thickness of the BAR, we utilize a thick BAR to reduce the FSR so that multiple acoustic modes can be accessed simultaneously. The BAR consists of a thin piezoelectric layer of c-axis-oriented AlN deposited on top of a thick oxidized high-resistivity Si substrate, which determines FSR $\approx (v_{\text{Si}}/2t) \approx 9.2$ MHz, where $v_{\text{Si}} = 9.2$ km/s is the longitudinal acoustic wave velocity in Si and $t = 500\ \mu$m is the thickness of Si. The maximum coupling strength can be achieved when the thickness of the piezoelectric layer matches half acoustic wavelength [36]. We therefore choose the thickness of the AlN layer to be $d = 550$ nm

to optimize the coupling strength at $(\omega_{bn}/2\pi) \approx 10$ GHz [23].

To optimize the electromechanical coupling strength, the electric field of the microwave mode should be confined around the piezoelectric layer with its lateral mode distribution matching that of the acoustic mode. Therefore, we design a planar superconducting LC resonator so that the AlN layer of the BAR can approach close proximity of the capacitor surface where the electric field is concentrated. A schematic of our device is shown in Fig. 1(b). The superconducting resonator is fabricated from a 50-nm-thick niobium titanium nitride (NbTiN) film (critical temperature $T_c \approx 13$ K) deposited on a 127-μm-thick sapphire substrate. The sapphire chip is then flipped over and suspended on top of the BAR using thin bonding spacers located at the four corners of the BAR. A tiny gap of a few microns is maintained between the sapphire and the AlN surfaces to minimize mechanical contact loss. Since the shape of our superconducting resonator resembles the ancient Greek symbol of a serpent eating its own tail, hereafter, we name it "Ouroboros".

An optical micrograph of the Ouroboros resonator is shown in Fig. 1(d). The structure is patterned using e-beam lithography with a hydrogen silsesquioxane (HSQ) resist followed by chlorine-based dry etching. The Ouroboros consists of a "capacitor" formed by a central circular pad and a surrounding "open-ring" pad, which are shunted by an "inductor" made of a long arc-shaped narrow wire. The parameters of the Ouroboros [labeled in Fig. 1(c)] are designed using finite element high-frequency simulation software (HFSS) to determine the microwave resonance to be $(\omega_a/2\pi) = 10$ GHz in presence of the dielectric loading of the BAR. When the Ouroboros is excited on resonance, electric field (E_z) is concentrated and tightly confined near the capacitor pad surfaces [Fig. 1(e)], improving the mode overlap in the z direction between the microwave mode and the AlN layer. Moreover, because of the $\delta v/v$ effect [38–40], the proximal capacitor modifies the acoustic wave velocity in the BAR and creates an effective potential well in the lateral direction just under the location of the capacitor, providing lateral confinement for the acoustic thickness modes. A detailed discussion on the $\delta v/v$-effect-induced acoustic mode bounding is beyond the scope of this article and will be presented elsewhere [41]. It is worth mentioning that another advantage of the Ouroboros design is that the long-arc inductor allows supercurrents to generate magnetic flux far extended from the chip surface, making it feasible to inductively couple the Ouroboros with an off-chip loop probe for microwave signal input and readout.

Strong coupling.—In order to experimentally investigate the coherent cavity piezoelectromechanical coupling, the device is encapsulated in a high-conductivity copper box and loaded in a closed-loop refrigerator with a base temperature of 1.62 K [42]. In all experiments, the power of the microwave probe signal is set to be below −60 dBm to avoid undesired nonlinear and heating effects in the superconducting resonator.

We first study the properties of the coupled system by probing the microwave reflection spectrum using a vector network analyzer. Figure 2(a) shows the amplitude and the phase spectra of the reflection coefficient S_{11} at 1.7 K. Several sharp resonance dips with distinct phase changes are clearly observed. Among all the resonances, the two most prominent dips at 10.171 GHz and 10.176 GHz are particularly close to each other [light blue area in Fig. 2(a)]. As the resonances become further away from these two center resonances, the mode spacing becomes more uniform and gradually approaches a constant of 9.1 MHz, which matches well with the calculated FSR of the acoustic thickness modes of the BAR. This implies that those "side bands" originate from thickness modes of different orders, whereas the Ouroboros resonance is mostly hybridized with a closely matched thickness mode ($n = n_0 \approx 1100$) to produce the two hybrid resonances at 10.171 GHz and 10.176 GHz. To better visualize the coupling induced frequency shifts, we measure the frequency difference between two far-separated resonances away from 10.173 GHz, and count the number of mechanical resonances between them. The ratio gives the FSR of the

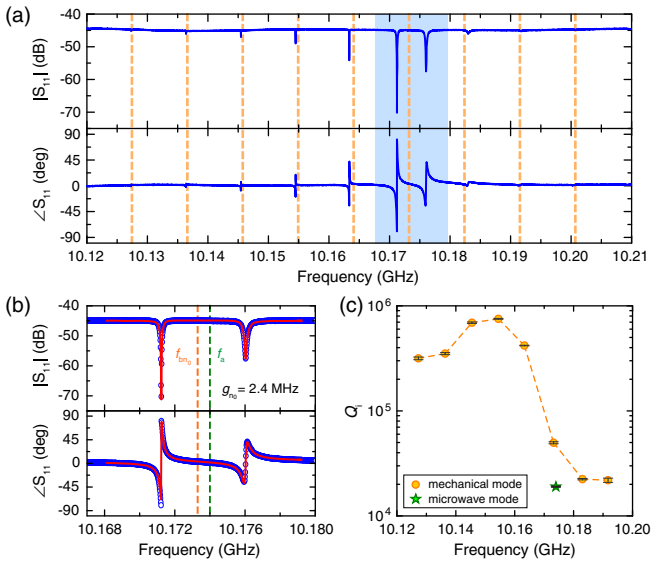

FIG. 2. (a) Microwave reflection spectrum of the device measured at 1.7 K. Orange dashed lines: Unperturbed frequencies of the acoustic thickness modes of the BAR. (b) Close-up spectrum of the regime where the microwave mode strongly hybridizes with the acoustic thickness modes. Red lines: Fittings using the coupled-mode formula. Green and orange dashed lines: Fitted center resonant frequencies of the uncoupled microwave mode $f_a = (\omega_a/2\pi)$ and the thickness mode $f_{bn_0} = (\omega_{bn_0}/2\pi)$, respectively. (c) Fitted intrinsic quality factors of the microwave mode and the different orders of acoustic thickness modes of the BAR.

thickness modes, which is found to be 9.12 MHz. Based on this measured FSR value, we overlay the unperturbed frequencies of thickness modes as vertical orange dashed lines in Fig. 2(a). It be can seen that the density of modes is mostly modified around the two resonances at 10.171 GHz and 10.176 GHz where the electromechanical coupling leads to strong hybridization of the microwave and the mechanical modes.

The spectra of the hybridized modes are fitted [Fig. 2(b)] by

$$S_{11}(\omega) = -1 + \frac{2\kappa_{a,e}}{-i(\omega-\omega_a)+\kappa_{a,i}+\kappa_{a,e}-\sum_n \frac{|g_n|^2}{i(\omega-\omega_{bn})-\kappa_{bn}}}, \tag{3}$$

which is the steady-state solution of the coupled-multimode formula. Here, $\kappa_{a,i}$ and $\kappa_{a,e}$ are the intrinsic dissipation rate and the external coupling rate of the Ouroboros, respectively. As expected, the fitted frequencies of the uncoupled microwave mode $(\omega_a/2\pi) = 10.1740$ GHz and the thickness mode $(\omega_{bn_0}/2\pi) = 10.1733$ GHz are very close to each other. The coupling strength is extracted to be $(g_{n_0}/2\pi) = 2.4$ MHz, larger than the dissipation rates of both the microwave mode $(\kappa_{a,i}+\kappa_{a,e}/2\pi) = 0.39$ MHz $((\kappa_{a,i}/2\pi) = 0.27$ MHz, $(\kappa_{a,e}/2\pi) = 0.12$ MHz) and the thickness mode $(\kappa_{bn_0}/2\pi) = 0.10$ MHz. Therefore, our system is in the strong coupling regime [14,15] and a cooperativity of $C = g_{n_0}^2/(\kappa_a\kappa_{bn_0}) \approx 148$ is obtained.

By this method, the intrinsic losses of all the thickness modes in the spectrum in Fig. 2(a) are extracted and the corresponding Q factors are plotted in Fig. 2(c). A highest mechanical Q factor of 7.5×10^5 is obtained, giving rise to an ultrahigh cooperativity of $C \approx 2178$. An important figure of merit quantifying the decoupling of a mechanical resonator from the thermal environment is the fQ product [1,43–45]. Our system exhibits a high fQ product of 7.5×10^{15} Hz at 1.7 K, more than 3 orders larger than previous experimental result [20]. This high fQ product translates to excellent coherence characterized by a large number of coherent oscillations given by $(hfQ/k_BT) \approx 2\times10^5$ in the presence of thermal decoherence. The asymmetry of the mechanical Q factors with respect to the Ouroboros resonant frequency can be attributed to the microwave cavity-mediated coupling between the localized thickness modes in the potential well and the unlocalized leaky modes [41].

Temperature dependence and frequency tuning.—The features of multimode strong coupling in our system are further investigated by gradually sweeping the Ouroboros resonant frequency via temperature tuning. When the temperature increases, the Ouroboros resonant frequency decreases monotonically due to the reduction of the density of Cooper pairs in the superconductor. Figure 3(a) shows the microwave reflection spectra with the temperature varying from 1.7 K to 7.5 K. As the Ouroboros resonant frequency is swept over several FSRs of the thickness modes, avoided crossings are observed in sequence as a signature of multimode strong coupling (MMSC) [28,46]. In Fig. 3(b), typical spectra at different temperatures are shown in the linear plot. It can be seen that at higher temperatures the coupled modes shift dramatically to lower frequencies with increased resonance linewidths and reduced dip extinctions due to increased internal dissipation.

Using the coupled-multimode model, the uncoupled Ouroboros resonant frequency at different temperatures is extracted and plotted as the blue dashed line in Fig. 3(a), which agrees with the kinetic inductance model of thin-film superconducting resonators [47]. The BAR mechanical resonant frequencies, on the other hand, shift less than 5 Hz because of the extremely small thermal expansion coefficient of silicon within the temperature range of our experiments [48]. Figure 3(c) shows the coupling strength and the intrinsic Q factors extracted at temperatures when the Ouroboros is on resonance with a thickness mode. In the temperature range we studied, g_n remains almost constant around 2.4 MHz. The intrinsic Q factor of the Ouroboros

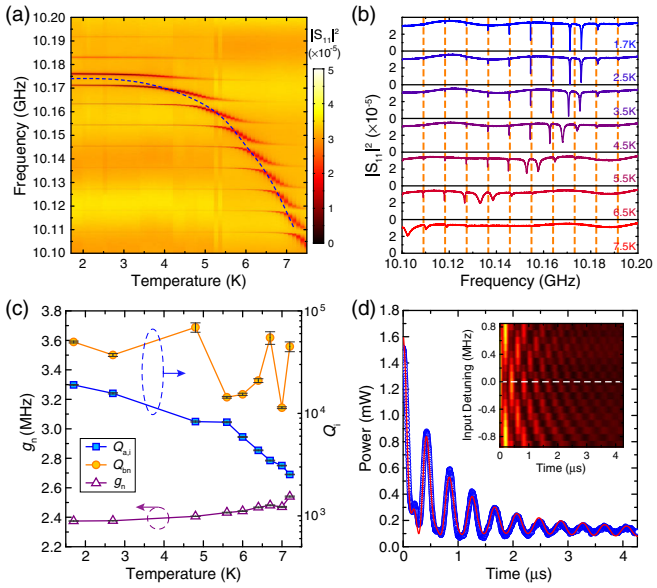

FIG. 3. (a) Temperature dependence of the microwave reflection spectra. Blue dashed line: The uncoupled Ouroboros resonant frequency obtained from the fittings using the coupled-mode formula. (b) Line plots of the microwave reflection spectra at different temperatures. Orange dashed lines: Unperturbed frequencies of the acoustic thickness modes of the BAR. (c) Coupling strength and intrinsic Q factors extracted at temperatures when the Ouroboros is on resonance with a thickness mode. (d) Microwave reflection in the time domain. The center frequency of the input microwave pulse is 10.1737 GHz. Red line: The fitting of the exponentially decaying oscillation with background signals. Inset: Temporal oscillations at different input frequencies detuned from 10.1737 GHz (white dashed line).

gradually drops due to the increasing quasiparticle dissipation, while the Q factors of the thickness modes show a general decreasing trend but with fluctuations, which could be attributed to property variations among different orders of modes.

Dynamics.—The strong coupling permits coherent energy exchange between coupled modes. We therefore study the dynamic interaction between the microwave and the mechanical modes in time domain. Experimentally, a short microwave excitation pulse is injected into the coupled system and the reflected power is amplified and monitored at 1.7 K. Periodical oscillations in the time domain are observed for input pulses with different center frequencies around 10.1737 GHz [inset of Fig. 3(d)], which is the average frequency between the Ouroboros and the closely coupled mechanical resonance. The oscillation trace at 10.1737 GHz is plotted in Fig. 3(d), corresponding to the white dashed line in Fig. 3(d), inset. It can be seen that because of the fast coherent energy exchange between the strongly coupled microwave and mechanical modes, the reflected power oscillates periodically with exponentially decaying amplitude. In experiments, the nonideal edge of the input pulse produces a decaying background which interferes and distorts the exponentially decaying oscillation. Taking into account the background terms, the time trace can be well fitted with the decaying signals of the two hybrid modes at 10.1712 GHz and 10.1760 GHz [red line in Fig. 3(d)], in excellent agreement with the frequency domain measurement. Fitting details are described in Ref. [36].

Conclusion.—We have achieved multimode electromechanical strong coupling between a superconducting microwave resonator and a piezoelectric BAR at 10 GHz with a cooperativity exceeding 2000. Coherent interaction has been demonstrated via the observation of the avoided-crossing spectra and the temporal oscillation of microwave energy. Because of the high operating frequency, our system can be expected to incorporate with quantum superconducting circuits for studying mechanical quantum states at relaxed refrigeration temperatures. The achieved ultrahigh fQ product of 7.5×10^{15} Hz and large coupling strength-over-FSR ratio of $(g_n/\mathrm{FRS}) \approx 26\%$ allow the realization of mechanical multimode quantum memory devices [27] and exploration of the intriguing superstrong coupling regime [28,30].

C. L. Z. thanks Liang Jiang for helpful discussions. This work is supported by Laboratory of Physical Sciences through a grant from Army Research Office (W911NF-14-1-0563), an Air Force Office of Scientific Research (AFOSR) MURI Grant (No. FA9550-15-1-0029), a US-Israel Binational Science Foundation Grant (No. 2012148) and an NSF MRSEC Grant (No. 1119826). H. X. T. acknowledges support from a Packard Fellowship in Science and Engineering. The authors thank Michael Power and Dr. Michael Rooks for assistance in device fabrication.

*hong.tang@yale.edu

[1] M. Aspelmeyer, T. J. Kippenberg, and F. Marquardt, Cavity optomechanics, Rev. Mod. Phys. **86**, 1391 (2014).
[2] C. A. Regal and K. W. Lehnert, From cavity electromechanics to cavity optomechanics, J. Phys. Conf. Ser. **264**, 012025 (2011).
[3] R. W. Andrews, R. W. Peterson, T. P. Purdy, K. Cicak, R. W. Simmonds, C. a. Regal, and K. W. Lehnert, Bidirectional and efficient conversion between microwave and optical light, Nat. Phys. **10**, 321 (2014).
[4] J. D. Teufel, T. Donner, D. Li, J. W. Harlow, M. S. Allman, K. Cicak, A. J. Sirois, J. D. Whittaker, K. W. Lehnert, and R. W. Simmonds, Sideband cooling of micromechanical motion to the quantum ground state, Nature (London) **475**, 359 (2011).
[5] J. Chan, T. P. M. Alegre, A. H. Safavi-Naeini, J. T. Hill, A. Krause, S. Gröblacher, M. Aspelmeyer, and O. Painter, Laser cooling of a nanomechanical oscillator into its quantum ground state, Nature (London) **478**, 89 (2011).
[6] R. W. Peterson, T. P. Purdy, N. S. Kampel, R. W. Andrews, P.-L. Yu, K. W. Lehnert, and C. A. Regal, Laser Cooling of a Micromechanical Membrane to the Quantum Backaction Limit, Phys. Rev. Lett. **116**, 063601 (2016).
[7] E. E. Wollman, C. U. Lei, A. J. Weinstein, J. Suh, A. Kronwald, F. Marquardt, A. A. Clerk, and K. C. Schwab, Quantum squeezing of motion in a mechanical resonator, Science **349**, 952 (2015).
[8] F. Lecocq, J. B. Clark, R. W. Simmonds, J. Aumentado, and J. D. Teufel, Quantum Nondemolition Measurement of a Nonclassical State of a Massive Object, Phys. Rev. X **5**, 041037 (2015).
[9] J. T. Hill, A. H. Safavi-Naeini, J. Chan, and O. Painter, Coherent optical wavelength conversion via cavity optomechanics, Nat. Commun. **3**, 1196 (2012).
[10] T. Bagci, A. Simonsen, S. Schmid, L. G. Villanueva, E. Zeuthen, J. Appel, J. M. Taylor, A. Sørensen, K. Usami, A. Schliesser, and E. S. Polzik, Optical detection of radio waves through a nanomechanical transducer, Nature (London) **507**, 81 (2014).
[11] R. W. Andrews, A. P. Reed, K. Cicak, J. D. Teufel, and K. W. Lehnert, Quantum-enabled temporal and spectral mode conversion of microwave signals, Nat. Commun. **6**, 10021 (2015).
[12] J. D. Teufel, D. Li, M. S. Allman, K. Cicak, a. J. Sirois, J. D. Whittaker, and R. W. Simmonds, Circuit cavity electromechanics in the strong-coupling regime, Nature (London) **471**, 204 (2011).
[13] E. Verhagen, S. Deléglise, S. Weis, A. Schliesser, and T. J. Kippenberg, Quantum-coherent coupling of a mechanical oscillator to an optical cavity mode, Nature (London) **482**, 63 (2012).
[14] X. Zhang, C.-L. Zou, L. Jiang, and H. X. Tang, Strongly Coupled Magnons and Cavity Microwave Photons, Phys. Rev. Lett. **113**, 156401 (2014).
[15] Y. Tabuchi, S. Ishino, T. Ishikawa, R. Yamazaki, K. Usami, and Y. Nakamura, Hybridizing Ferromagnetic Magnons and Microwave Photons in the Quantum Limit, Phys. Rev. Lett. **113**, 083603 (2014).
[16] M. Poggio, C. L. Degen, H. J. Mamin, and D. Rugar, Feedback Cooling of a Cantilever's Fundamental Mode below 5 mK, Phys. Rev. Lett. **99**, 017201 (2007).

[17] K. H. Lee, T. G. McRae, G. I. Harris, J. Knittel, and W. P. Bowen, Cooling and Control of a Cavity Optoelectromechanical System, Phys. Rev. Lett. **104**, 123604 (2010).
[18] T. A. Palomaki, J. D. Teufel, R. W. Simmonds, and K. W. Lehnert, Entangling Mechanical Motion with Microwave Fields, Science **342**, 710 (2013).
[19] C. Xiong, L. Fan, X. Sun, and H. X. Tang, Cavity piezooptomechanics: Piezoelectrically excited, optically transduced optomechanical resonators, Appl. Phys. Lett. **102**, 021110 (2013).
[20] A. D. O'Connell, M. Hofheinz, M. Ansmann, R. C. Bialczak, M. Lenander, E. Lucero, M. Neeley, D. Sank, H. Wang, M. Weides, J. Wenner, J. M. Martinis, and a. N. Cleland, Quantum ground state and single-phonon control of a mechanical resonator, Nature (London) **464**, 697 (2010).
[21] J. Bochmann, A. Vainsencher, D. D. Awschalom, and A. N. Cleland, Nanomechanical coupling between microwave and optical photons, Nat. Phys. **9**, 712 (2013).
[22] X. Han, C. Xiong, K. Y. Fong, X. Zhang, and H. X. Tang, Triply resonant cavity electro-optomechanics at X-band, New J. Phys. **16**, 063060 (2014).
[23] X. Han, K. Y. Fong, and H. X. Tang, A 10-GHz film-thickness-mode cavity optomechanical resonator, Appl. Phys. Lett. **106**, 161108 (2015).
[24] J. D. Cohen, S. M. Meenehan, G. S. MacCabe, S. Gröblacher, A. H. Safavi-Naeini, F. Marsili, M. D. Shaw, and O. Painter, Phonon counting and intensity interferometry of a nanomechanical resonator, Nature (London) **520**, 522 (2015).
[25] K. C. Balram, M. I. Davanço, J. D. Song, and K. Srinivasan, Coherent coupling between radiofrequency, optical and acoustic waves in piezo-optomechanical circuits, Nat. Photonics **10**, 346, (2016).
[26] D. O. Krimer, M. Liertzer, S. Rotter, and H. E. Türeci, Route from spontaneous decay to complex multimode dynamics in cavity QED, Phys. Rev. A **89**, 033820 (2014).
[27] X. Zhang, C.-l. Zou, N. Zhu, F. Marquardt, L. Jiang, and H. X. Tang, Magnon dark modes and gradient memory, Nat. Commun. **6**, 8914 (2015).
[28] N. M. Sundaresan, Y. Liu, D. Sadri, L. J. Szőcs, D. L. Underwood, M. Malekakhlagh, H. E. Türeci, and A. A. Houck, Beyond Strong Coupling in a Multimode Cavity, Phys. Rev. X **5**, 021035 (2015).
[29] N. Kostylev, M. Goryachev, and M. E. Tobar, Superstrong coupling of a microwave cavity to yttrium iron garnet magnons, Appl. Phys. Lett. **108**, 062402 (2016).
[30] X. Zhang, C. Zou, L. Jiang, and H. X. Tang, Superstrong coupling of thin film magnetostatic waves with microwave cavity, J. Appl. Phys. **119**, 023905 (2016).
[31] J. Stettenheim, M. Thalakulam, F. Pan, M. Bal, Z. Ji, W. Xue, L. Pfeiffer, K. W. West, M. P. Blencowe, and A. J. Rimberg, A macroscopic mechanical resonator driven by mesoscopic electrical back-action, Nature (London) **466**, 86 (2010).
[32] M. Schmidt, M. Ludwig, and F. Marquardt, Optomechanical circuits for nanomechanical continuous variable quantum state processing, New J. Phys. **14**, 125005 (2012).
[33] H. Seok, L. F. Buchmann, E. M. Wright, and P. Meystre, Multimode strong-coupling quantum optomechanics, Phys. Rev. A **88**, 063850 (2013).
[34] A. Frangi, M. Cremonesi, A. Jaakkola, and T. Pensala, Analysis of anchor and interface losses in piezoelectric MEMS resonators, Sens. Actuators **190**, 127 (2013).
[35] L.-W. Hung and C. T. -C. Nguyen, Capacitive-piezoelectric transducers for high-Q micromechanical AlN resonators, J. Microelectromech. Syst. **24**, 458 (2015).
[36] See Supplemental Material at http://link.aps.org/supplemental/10.1103/PhysRevLett.117.123603 for the calculation and estimation of the coupling strength, and the fittings of the temporal oscillations.
[37] C.-L. Zou, X. Han, L. Jiang, and H. X. Tang, Cavity piezomechanical strong coupling and frequency conversion on an aluminum nitride chip, Phys. Rev. A **94**, 013812 (2016).
[38] A. Yamada and H. Shimizu, Accurate analysis of $\delta v/v$ surface acoustic waveguides on a piezoelectric anisotropic substrate, Electron. Commun. Jpn. 1, Commun. **70**, 38 (1987).
[39] A. J. Hughes, Elastic surface wave guidance by $(\delta v/v)$ effect guidance structures, J. Appl. Phys. **43**, 2569 (1972).
[40] A. N. Nordin, Ph.D. thesis, George Washington University, 2008.
[41] C.-L. Zou, X. Han, L. Jiang, and H. X. Tang, Strong piezomechanical coupling induced acoustic mode trapping (to be published).
[42] C. Wang, B. Lichtenwalter, A. Friebel, and H. X. Tang, A closed-cycle 1K refrigeration cryostat, Cryogenics **64**, 5 (2014).
[43] D. E. Chang, K.-K. Ni, O. Painter, and H. J. Kimble, Ultrahigh-Q mechanical oscillators through optical trapping, New J. Phys. **14**, 045002 (2012).
[44] M. Goryachev, D. L. Creedon, E. N. Ivanov, S. Galliou, R. Bourquin, and M. E. Tobar, Extremely low-loss acoustic phonons in a quartz bulk acoustic wave resonator at millikelvin temperature, Appl. Phys. Lett. **100**, 243504 (2012).
[45] S. Galliou, M. Goryachev, R. Bourquin, P. Abbé, J. P. Aubry, and M. E. Tobar, Extremely low loss phonon-trapping cryogenic acoustic cavities for future physical experiments, Sci. Rep. **3**, 2132 (2013).
[46] A. Noguchi, R. Yamazaki, M. Ataka, H. Fujita, Y. Tabuchi, T. Ishikawa, K. Usami, and Y. Nakamura, Strong coupling in multimode quantum electromechanics, arXiv:1602.01554.
[47] J. Gao, Ph.D. thesis, California Institute of Technology, 2008.
[48] C. A. Swenson, Recommended values for the thermal expansivity of silicon from 0 to 1000 K, J. Phys. Chem. Ref. Data **12**, 179 (1983).